https://doi.org/10.1016/j.optcom.2021.127314

Mode Analysis of Orbital Angular Momentum Modes Carrying Multi-Mode Ring-Core Fibers

Jiajing Tu[a,*], Quanchao Lu[b], Zhuo Wang[c], Shecheng Gao[a], Weiping Liu[a], Changyuan Yu[c], Zhaohui Li[b], Chao Lu[c]

[a] *Department of Electronic Engineering, School of Information Science and Technology, Jinan University, Guangzhou 510632, China*
[b] *State Key Lab Optoelectric Material and Technology, School of Electric and Information Technology, Sun Yat Sen University, Guangzhou 510275, Guangdong, China*
[c] *Department of Electronic and Information Engineering, The Hong Kong Polytechnic University, Hong Kong, China*

Abstract

We discuss the mode properties for orbital angular momentum (OAM) modes supporting multi-mode ring-core fiber (MM-RCF). For the strongly-guiding MM-RCF, by introducing one more layer to the ring-core, a two-layer ring-core fiber (TL-RCF) is proposed. It is proved that this TL-RCF can increase the separation degree between vector eigenmodes and meanwhile weaken the spin-orbital coupling. For the mode group supporting MM-RCF, the maximum mode number is limited by the thickness of ring-core and the cut-off of radial higher-order mode. We also present the tradeoff relationship between mode group effective index difference and differential mode delay of vector eigenmodes in the mode group. The discussion in this paper can give guidance for the design of MM-RCF.

Keywords: Space division multiplexing, mode analysis, orbital angular momentum, ring-core fiber

2021 MSC: 00-01, 99-00

*Corresponding author
Email address: tujiajing@jnu.edu.cn (Jiajing Tu)

1. Introduction

As space division multiplexing (SDM) technologies, multi-mode fiber (MMF) as well as multi-core fiber (MCF) are two promising approaches to break through the capacity crunch of the traditional single-mode fiber transmission system, which has attracted intensive attention for decades [1–3]. Compared to MCF, MMF is a more integrated approach to increase the transmission channels. In a weakly-guiding MMF, vector eigenmodes have similar propagation constants, therefore linearly polarized (LP) mode will be formed due to the strongly mode coupling among these degenerated vector eigenmodes. Interestingly, two vector eigenmodes with identical propagation constants combining with $\pi/2$ phase shift will form a new pattern of mode with helical wave front, which is called orbital angular momentum (OAM) mode [4–6]. OAM mode supporting fibers used for optical communication usually carry radial first-order mode and each mode has similar mode pattern, while LP mode supporting fiber also has radial higher-order mode and each mode field distribution is different. Hence, compared to LP mode, the OAM mode based multiplexer/demultiplexer only need to regulate one layer of phase [7] and the OAM mode erbium doped fiber amplifier (EDFA) could have smaller differential mode gain (DMG), which is easier to achieve gain equalization [8].

In order to suppress the radial higher-order mode, OAM mode supporting fiber usually have depressed-inner region inside the core, which forms a ring shape of core [9, 10]. According to the separation degree of cylindrical vector (CV) eigenmodes, the OAM mode fiber can be divided into two categories. The first type is called strongly-guiding fiber, which is named relatively to the weakly-guiding fiber. If the core has very high up-doping concentration and low depressed part inside the core, the fiber will stay in a strongly-guiding condition, where CV eigenmodes in the same order will not be degenerated anymore and transmit as independent channels. C. Brunet et al. presented effective theoretical design tools for the strongly-guiding ring-core fiber [9]. B. Ung et al. proposed an inverse-parabolic graded-index fiber and proved that this special

structure could separate TE_{01},TM_{01}, and HE_{21} modes effectively [11]. In order to enlarge relative refractive index between the core and cladding (Δ_{co}) to a large extent, an air-hole is introduced into the ring-core and it has been proven that large isolation of the CV eigenmodes can be achieved[12, 13]. Besides the solid up-doping ring-core fiber, photonics crystal fiber (PCF) is another good candidate to obtain large separation between the CV eigenmodes in the same order, because the Δ_{co} can be easily adjusted by changing the relative air-hole size in the cladding[14–16]. The other type of OAM-carrying fiber is the traditional weakly-guiding fiber, in which CV eigenmodes in the same order are degenerated. Each mode group has fixed four modes except the 0^{th} order of OAM mode (OAM_{01} doesn not carry OAM). Therefore, even if the four modes are strongly-coupled, we can take advantage of fixed 4×4 multiple-input multiple-out digital signal processing (MIMO-DSP) to demultiplex the signals inside the mode group and detect each mode group directly. L. Zhu et al. presented 2.6-km MMF transmission using four data-carrying OAM mode groups (OAM_{01}, OAM_{11}^{+}/OAM_{11}^{-}, OAM_{21}^{+}, OAM_{31}^{+}) [17]. J. Zhang et al. adopted 4×4 MIMO processing to achieve an aggregate capacity of 2.56 Tbit/s and an overall spectral efficiency of 10.24 bit/(s·Hz) [18].

This paper will focus on the mode analysis for the above-mentioned two types of OAM-carrying fibers. We will reveal how the refractive index profile influence the mode properties by the numerical calculation and then present the design suggestion for each kind of fiber.

2. OAM-Carrying Fiber Modeling

For the step-index fiber, if the mode number increases, the radial higher-order modes will easily appear. However, the radial higher-order modes should not be included in the OAM-carrying fiber, because they will cause large crosstalk in the multiplexing/demultiplexing process [9]. Therefore, the refractive index profile need to be modified to suppress the undesired radial higher-order modes.

If we introduce perturbation of refractive index into the core (Δn), the propagation constant (β) can be expressed as follow [19]

$$\beta \approx \overline{\beta} + k\frac{\iint_A \Delta n|\overline{e}|^2 dA}{\iint_A |\overline{e}|^2 dA}, \tag{1}$$

where $\overline{\beta}$, and $\overline{e}$ are propagation constant and electric field distribution of the standard step-index fiber. k and A represent the free-space wavenumber and electric field area. Fig. 1(a) shows the normalized electric fields of HE_{11}, HE_{21}, HE_{31}, HE_{12}, and HE_{41} modes, respectively. We can find that radial higher-order mode HE_{12} has electrical field distribution at the center of core while other radial first-order modes do not have such part. If a perturbation of Δn is introduced inside the core, the propagation constant of radial higher-order mode can be regulated. Therefore, a ring-core structure was proposed to adjust the effective index (n_{eff}) and the size of the depressed part at the center has impact on n_{eff} of modes, especially the radial higher-order mode. Fig. 1(b) illustrates the dependence of normalized propagation constant (b) on the ratio (ρ) of inner radius (a) and outer radius (d) of the ring-core as shown in Fig. 1(c). In Fig. 1(b), $b = \frac{n_{\text{eff}}^2 - n_0^2}{n_1^2 - n_0^2}$ and $\rho = \frac{a}{d}$, where refractive index of core (n_1), refractive index of cladding (n_0), outer radius of ring-core (d) and operating wavelength (λ) are set as 1.480, 1.444, 8 μm, and 1550 nm, respectively. As shown in Fig. 1(b), it is obvious that the normalized propagation constant of HE_{12} mode (shown as red solid line with asterisk) decreases to a large extent as the ring-core is getting thinner and thinner. When ρ becomes larger than 0.69, the radial second-order mode HE_{12} can be cut off. This figure explains why the OAM-carrying fiber usually has ring-type core.

For the ring-core fiber, traditional expressions of electromagnetic field components in step-index fiber are not suitable any more. In order to obtain the β, we rewrite the expression of E_z and H_z for ring-core fiber as Eq. (2) and Eq. (3), where $A_1 \sim A_4$, $B_1 \sim B_4$ represent unknown amplitude coefficients and r is the radial coordinate. I_l and K_l are l^{th}-order first kind modified Bessel function and l^{th}-order second kind modified Bessel function. Since functions I_l and K_l converge at $r = 0$ μm and $r = \infty$, respectively, we set the z components

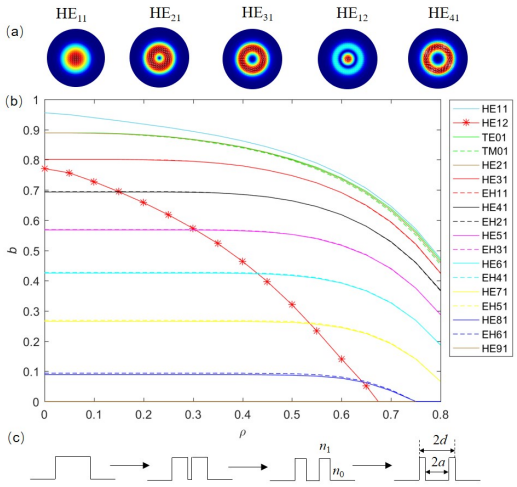

Figure 1: (a) Normalized electric filed of HE_{11}, HE_{21}, HE_{31}, HE_{12}, HE_{41} modes, (b) dependence of b on ρ, where n_1, n_0, d and λ are set as 1.480, 1.444, 8 μm, and 1550 nm, respectively, and (c) the evolvement of refractive index profile of ring-core with ρ getting larger.

of electromagnetic field as I_l and K_l, respectively at the domain of $r \leq a$ and $r > d$. J_l and N_l stand for l^{th}-order Bessel function and l^{th}-order Neumann function, respectively. $J_l + N_l$ is the proper solution in the ring-core. W_1 and U_1 are normalized transverse wave numbers in cladding and ring-core and can be expressed as $W_1 = d\sqrt{\beta^2 - k^2 n_0^2}$ and $U_1 = d\sqrt{k^2 n_1^2 - \beta^2}$, where k is the wave number in vacuum. Eq. (4) and Eq. (5) are the expression of E_θ and H_θ, where ω, μ_0, and ϵ_0 are angular frequency, permeability, and permittivity, respectively. Applying the boundary conditions that E_z, H_z, E_θ, and H_θ should be continuous at the interface $r = a$ and $r = d$ [20], we can obtain homogeneous system of 8 linear equations. We can calculate the corresponding β value for each mode in l^{th} order by making the square matrix containing $A_1 \sim A_4$ and $B_1 \sim B_4$ equal 0. Finally, $A_1 \sim A_4$ and $B_1 \sim B_4$ can be obtained.

$$E(z) = \begin{cases} A_1 I_l(r\frac{W_1}{d})\cos(l\theta + \phi) & r \leq a \\ \left[A_2 J_l(r\frac{U_1}{d}) + A_3 N_l(r\frac{U_1}{d})\right]\cos(l\theta + \phi) & a < r \leq d \\ A_4 K_l(r\frac{W_1}{d})\cos(l\theta + \phi) & r > d \end{cases} \tag{2}$$

$$H(z)=\begin{cases} B_1 I_l(r\frac{W_1}{d})\sin(l\theta+\phi) & r\le a \\ \left[B_2 J_l(r\frac{U_1}{d})+B_3 N_l(r\frac{U_1}{d})\right]\sin(l\theta+\phi) & a<r\le d \\ B_4 K_l(r\frac{W_1}{d})\sin(l\theta+\phi) & r>d \end{cases} \tag{3}$$

$$E(\theta)=-\frac{j}{k^2n^2(r)-\beta^2}\left[\frac{\beta}{r}\frac{\partial E_z}{\partial\theta}-\omega\mu_0\frac{\partial H_z}{\partial r}\right]. \tag{4}$$

$$H(\theta)=-\frac{j}{k^2n^2(r)-\beta^2}\left[\frac{\beta}{r}\frac{\partial H_z}{\partial\theta}-\omega\epsilon_0 n^2(r)\frac{\partial E_z}{\partial r}\right]. \tag{5}$$

Fig. 2(a) and Fig. 2(b) show absolute effective index difference between CV eigenmodes ($|\Delta n_{\mathrm{eff,CV}}|$) and absolute effective index difference between adjacent mode groups ($|\Delta n_{\mathrm{eff,MG}}|$) dependence on ρ. Here, all the structure parameters have the same setting with Fig. 1(b) and all the n_{eff} values were quickly calculated by using above-mentioned theoretical tool. In Fig. 2(a), we can find that $|\Delta n_{\mathrm{eff,CV}}|$ among HE_{21}, TE_{01}, and TM_{01} modes increase with ρ, while $|\Delta n_{\mathrm{eff,CV}}|$ between azimuthal higher-order HE and EH modes in the same OAM order group will decrease firstly and then increase, which is because the Y-axis in Fig. 1(a) is calculated by $|n_{\mathrm{eff,HE}}-n_{\mathrm{eff,EH}}|$, so n_{eff} of HE mode is firstly larger than that of EH mode and then becomes smaller than that of EH mode. In Fig. 2(b), it can be found that the thickness of the ring-core has bigger impact on $|\Delta n_{\mathrm{eff,MG}}|$ between the azimuthal low-order mode groups than that between the azimuthal higher-order mode groups.

From a theoretical perspective, the correction terms of propagation constants ($\delta\beta$) for the radial first-order CV eigenmodes can be expressed as Tab. 1 [21], where C_1 and C_2 can be given by Eq. (6) and Eq. (7). In Eq. (6) and Eq. (7), r is radial coordinate, r_0 is the radius of core, l is the topological charge which represent the azimuthal order of CV eigenmode, $E_l(r)$ is the electrical field distribution, $n(r)$ is the refractive index distribution in radial direction. When the ring-core becomes thinner, the electrical field at the index discontinuities will get high. Thus, $\frac{\partial E_l(r)}{\partial r}$ and $E_l(r)$ is getting larger at index step as the ρ becomes larger. The propagation constant of a mode represents phase accumulation and phase shift is mainly attribute to incident wave's

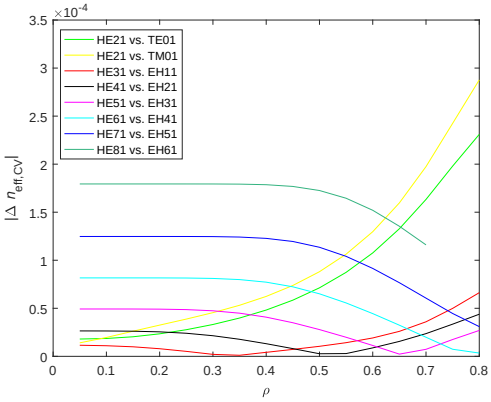

(a)

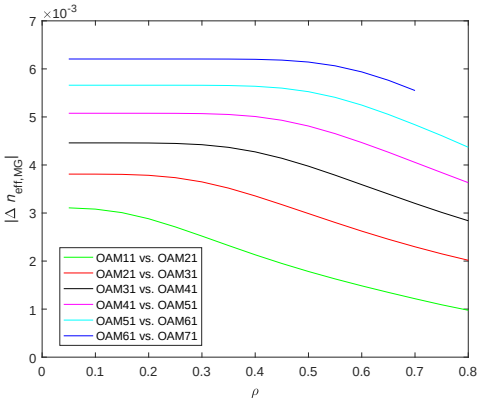

(b)

Figure 2: (a) $|\Delta n_{\mathrm{eff,CV}}|$ between CV eigenmodes and (b) $|\Delta n_{\mathrm{eff,MG}}|$ between adjacent mode groups dependence on ρ, where n_1, n_0, d and λ are set as 1.480, 1.444, 8 μm, and 1550 nm, respectively.

polarization orientation at the index discontinuities [10]. Thus, this explain why HE_{21}, TE_{01}, and TM_{01} modes have larger and larger separation as the ring-core is getting thinner in Fig. 2(a). Fig. 3(a) shows the electrical filed distribution of CV eigenmodes with $l \geq 2$ in a ring-core fiber, where refractive index of core is 1.480, refractive index of cladding is 1.444, outer radius of ring-core is 8 μm, inner radius of ring-core is 5.36 μm ($\rho = 0.67$), wavelength is 1550 nm. Electrical fields $E(r)$ of HE and EH mode are very close, which results in similar value of C_1 for these two CV eigenmodes. Thus, $\delta\beta$ between HE and EH mode are decided by C_2, whose numerator can be rewritten as $\int_0^{+\infty}[(E_l^2(r)\frac{\partial n^+(r)}{\partial r})|_{r=5.36} + (E_l^2(r)\frac{\partial n^-(r)}{\partial r})|_{r=8.00}]dr$. $\delta\beta$ between $HE_{l+1,1}$ and $EH_{l-1,1}$ can approximate to $-2C_2$. Fig. 3(b) enlarges the electrical field distribution of ring-core part in Fig. 3(a) and difference between the $E_l^2(r)$ at upward index step $r = 5.36$ μm and that at downward index step $r = 8.0$ μm represents the C_2. C_2 values of CV eigenmodes with $l = 2, 3$ are positive, C_2 values of CV eigenmodes with $l = 4$ is 0, and C_2 values of CV eigenmodes with $l = 5$, 6 are negative, which explains that n_{eff} of EH mode is larger than that of HE mode for $l = 2, 3$, n_{eff} of EH mode equals to that of HE mode for $l = 4$, and n_{eff} of HE mode is larger than that of EH mode for $l = 5, 6$ at $\rho = 0.67$ in Fig. 2(a).

There are two kinds of multi-mode ring-core fibers (MM-RCF), which are strongly-guiding MM-RCF and mode group supporting MM-RCF. Fig. 4 shows an concept figure for these two types of MM-RCF that can at most support $OAM_{l,m}$ with topological charge $l = 3$, radial order $m = 1$. For the strongly-guiding MM-RCF shown in Fig. 4(a), all the CV eigenmodes are separated with large Δn_{eff}. Because TE_{01} and TM_{01} are isolated, OAM mode formed by TE_{01} and TM_{01} is not stable. Therefore, OAM mode with $l = 1$ only contain the mode with a circular polarization in the same direction as the field rotation. Hence, 5 OAM modes can be used as independent channels and detected directly. If 2×2 MIMO-DSP is adopted, 10 states of OAM modes can be obtained for strongly-guiding MM-RCF shown in Fig. 4(a). For the mode group supporting ring-core fiber, the CV eigenmodes are still under the degenerated condition but the mode group in each order are well-separated. Therefore, we

can detect 3 mode groups directly and 12 states of OAM modes can be obtained for mode-group supporting MM-RCF shown in Fig. 4(b) by using 4×4 MIMO-DSP. In the following section, we will discuss the mode properties of these two types of MM-RCF.

Table 1: Modified propagation constant for each CV eigenmode.

CV eigenmode	$\delta\beta$
$\mathrm{HE}^{\mathrm{even}}_{l+1,1}$,$\mathrm{HE}^{\mathrm{odd}}_{l+1,1}$ $(l=0)$	C_1
$\mathrm{TE}_{0,1}$	0
$\mathrm{TM}_{0,1}$	$2(C_1+C_2)$
$\mathrm{HE}^{\mathrm{even}}_{l+1,1}$,$\mathrm{HE}^{\mathrm{odd}}_{l+1,1}$ $(l\geq 1)$	C_1-C_2
$\mathrm{EH}^{\mathrm{even}}_{l-1,1}$,$\mathrm{EH}^{\mathrm{odd}}_{l-1,1}$ $(l\geq 2)$	C_1+C_2

$$C_1=\frac{\Delta}{2kn_1r_0^2}\frac{\int_0^{+\infty} rE_l(r)\frac{\partial E_l(r)}{\partial r}\frac{\partial n(r)}{\partial r}dr}{\int_0^{+\infty} rE_l^2(r)dr}. \tag{6}$$

$$C_2=\frac{l\Delta}{2kn_1r_0^2}\frac{\int_0^{+\infty} E_l^2(r)\frac{\partial n(r)}{\partial r}dr}{\int_0^{+\infty} rE_l^2(r)dr}. \tag{7}$$

3. Strongly-Guiding MM-RCF

By observing Tab.1, Eq. (6) and Eq. (7), we can find that if more index steps are introduced into the refractive index profile of ring-core, then more $\frac{\partial n(r)}{\partial r}$ components will be added in the numerator of Eq. (6) and Eq. (7). As a result, the Δn_{eff} between the HE and EH modes may increase. Here, we adjust the refractive index of ring-core in Fig. 5(b) partially. n_{max} means the maximum of refractive index we set for core, which is fixed at 1.480 for the calculation. n_{ch} represents the refractive index part that we adjust. If we increase the n_{ch} from n_{max}, a new ring-core structure with dual index-steps at outer edge will be formed as shown in Fig. 5(a). If we decrease the n_{ch} from n_{max}, another new ring-core structure with dual index-steps at inner edge will be formed as

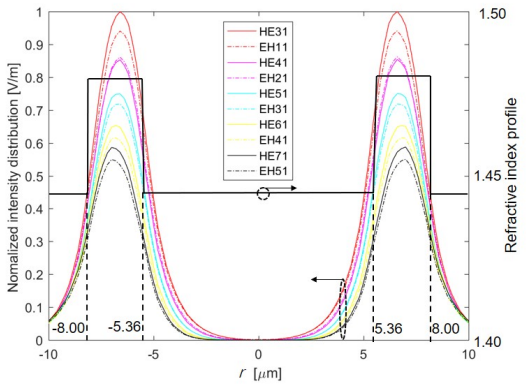

(a)

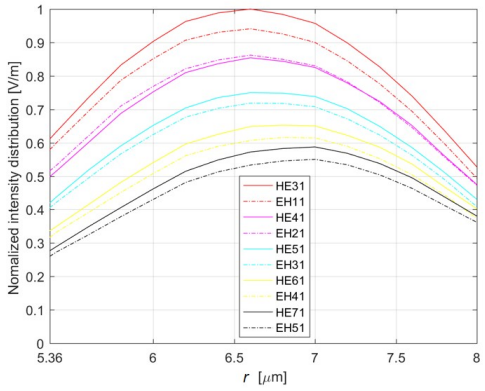

(b)

Figure 3: (a) Electrical filed distribution of CV eigenmodes with $l \geq 2$ in a step-index ring-core fiber, where refractive index of core is 1.480, refractive index of cladding is 1.444, outer radius of ring-core is 8 μm, inner radius of ring-core is 5.36 μm ($\rho = 0.67$), and wavelength is 1550 nm, and (b) enlarged ring-core part in Fig. 3(a).

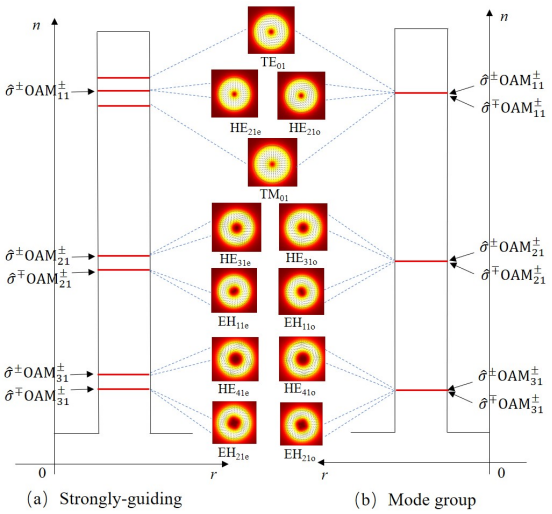

Figure 4: Concept figure for (a) strongly-guiding ring-core fiber and (b) mode group supporting ring-core fiber.

shown in Fig. 5(c). In Fig. 5, a_1, a_2, and a_3 represent the distance from the centre of core to the inner index-step edge, the middle index-step edge, and the outer index-step edge of ring-core, respectively. n_{cl} and n_{de} stand for refractive indices of cladding and inner depressed part.

Fig. 6 shows how n_{ch} influences the $|\Delta n_{\mathrm{eff,CV}}|$ when (a) n_{de} =1.0, (b) n_{de}= 1.42, and (c) n_{de} = 1.444, where n_{max}, n_{ch}, λ, a_2/a_3, a_1/a_3 are 1.480, 1.444, 1550 nm, 0.8, 0.67, respectively. Take Fig. 6(b) as example, when we adjust n_{ch} from n_{max} of 1.480, $|\Delta n_{\mathrm{eff,CV}}|$ in the OAM mode group of l = 1, 2, 3, 4 will increase, where $|\Delta n_{\mathrm{eff,CV}}| = n_{\mathrm{eff,HE}} - n_{\mathrm{eff,EH}}$ and $n_{\mathrm{eff,HE}}$ is always larger than $n_{\mathrm{eff,EH}}$. That $|\Delta n_{\mathrm{eff,CV}}|$ in OAM$_{61}$ and OAM$_{71}$ has point of inflection is because the sign of $\Delta n_{\mathrm{eff,CV}}$ changes at that point. Comparing Fig. 6(a), 6(b), and 6(c), we can find that large relative refractive index between core and cladding can lift the $|\Delta n_{\mathrm{eff,CV}}|$ for $n_{\mathrm{eff,HE}}$>$n_{\mathrm{eff,EH}}$ case. Fig. 7 illustrates $|\Delta n_{\mathrm{eff,MG}}|$ dependence on n_{ch}. We can find that changing n_{ch} will not affect the $|\Delta n_{\mathrm{eff,MG}}|$ very much and the variation is not larger than 2×10^{-3} if n_{ch} shifts from 1.42 to 1.50. Furthermore, we can also know that lower n_{de} can obtain

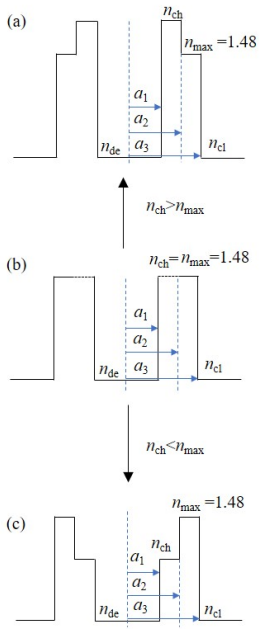

Figure 5: (a) Ring-core structure with dual index-steps at outer edge, (b) original ring-core structure, and (c) ring-core structure with dual index-steps at inner edge.

higher $|\Delta n_{\mathrm{eff,MG}}|$.

As shown in Fig. 6, smaller n_{de} can enlarge the relative refractive index between core and cladding, so $|\Delta n_{\mathrm{eff,CV}}|$ in Fig. 6(a) is larger than those in Figs. 6(b) and 6(c). Because large Δ_{co} break the weakly-guiding approximation of wave equation, so CV eigenmodes can be well separated. However, large Δ_{co} between core and cladding will introduce the intrinsic crosstalk. x and y components of OAM mode are expressed as Eq. (8) and Eq. (9), where superscript $\pm$ represents the right and left rotation of wavefront. Here, s is a constant and is defined as $\frac{\omega\mu_0 C}{\beta A}$, where ω, μ_0, C, β and A are angular frequency of the sinusoidally varying electromagnetic fields, permeability, light velocity in a vacuum, propagation constant, and undetermined coefficient, respectively. $P(r) = \frac{1}{2}[\frac{\partial F_{lz}(r)}{\partial r} + \frac{1}{r}F_{lz}(r)]$, and $Q(r) = \frac{1}{2}[\frac{\partial F_{lz}(r)}{\partial r} - \frac{1}{r}F_{lz}(r)]$, where $F_{lz}(r)$ means radial dependence of the field profile and l is the mode order. Hence, the expression of OAM mode can be expressed as Eq. (10), where $\vec{x}$ and $\vec{y}$ are two orthogonal unit vectors in Cartesian coordinate, $\hat{\sigma}^{\pm}$ stands for the right-handed and left-handed circular polarization. In Eq. (10), we can find that OAM mode consists of two parts, in which one part are the mode of $(l+1)$ with circular polarization in the opposite direction as the field rotation and the other part are the mode of $(l-1)$ with circular polarization in the same direction as the field rotation. In the weakly-guiding approximation condition, $|s|$ is close to 1, so the OAM mode only has a single component with a single topological charge number, which indicates high mode purity. When the weakly-guiding condition is broken by enlarging the relative refractive index between core and cladding, in other words, $|s| \neq 1$, two modes with topological charge difference of 2 will form a OAM mode. Fig. 8(a) shows normalized intensity distribution of OAM mode formed by even and odd HE_{31} vector modes with $\pi/2$ phase shift in a strongly-guiding hollow-ring-core fiber. Here, inner core radius is 6.4 μm, outer core radius is 8 μm, ring-core refractive index is 1.480, and refractive index of cladding is 1.444. It is obvious that this formed OAM mode has two OAM components as shown in Figs. 8(b) and 8(c), which are mode with $l = +2$ in right-handed circular polarization (RCP) and the other mode with $l = +4$ in

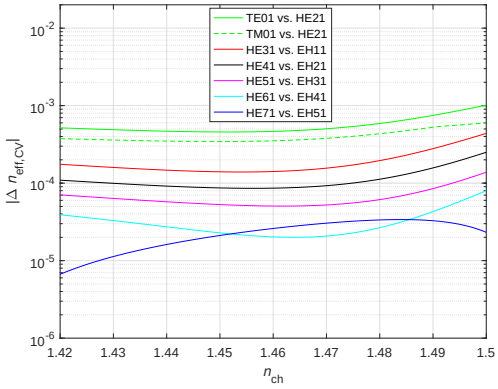

(a)

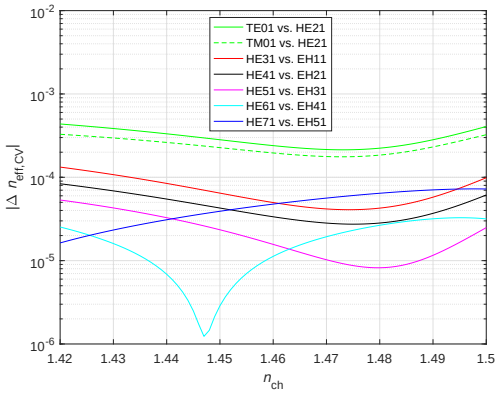

(b)

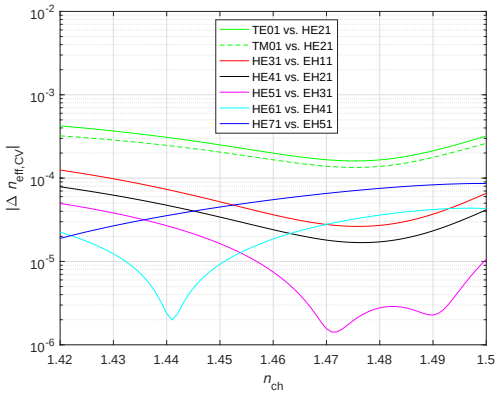

(c)

Figure 6: Dependence of $|\Delta n_{\mathrm{eff,CV}}|$ between CV eigenmodes on n_{ch} for (a) $n_{\mathrm{de}} = 1.0$, (b) $n_{\mathrm{de}} = 1.42$, and (c) $n_{\mathrm{de}} = 1.444$, where n_{max}, n_{ch}, λ, a_2/a_3, a_1/a_3 are 1.480, 1.444, 1550 nm, 0.8, 0.67, respectively.

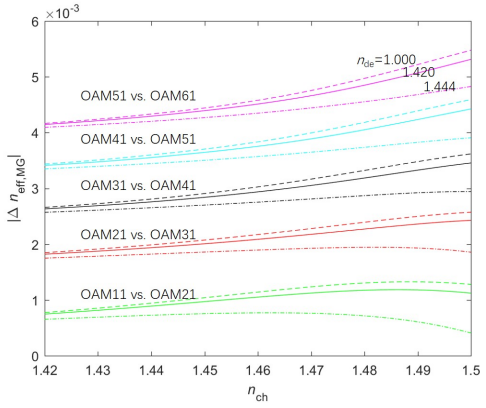

Figure 7: Dependence of $|\Delta n_{\mathrm{eff,MG}}|$ between OAM mode group on n_{ch} for $n_{\mathrm{de}} = 1.0$, 1.42, and 1.444, where $n_{\max}$, n_{ch}, λ, a_2/a_3, a_1/a_3 are 1.480, 1.444, 1550 nm, 0.8, 0.67, respectively.

left-handed circular polarization (LCP). This means that if a OAM mode with single topological is input into a strongly-guiding fiber with very thin ring-core, another OAM mode will be excited, which cause a spin-orbit coupling [22, 23]. Because this crosstalk is caused by the fiber structure, so we usually call it intrinsic crosstalk. What we can learn from this phenomenon is that we should avoid large discontinuity in the refractive index profile and very thin ring-core when we design OAM carrying ring-core fiber.

$$\begin{aligned} OAM_x^{\pm} = &- \frac{j\beta A}{[k^2 n(r)^2 - \beta^2]}[(1+s)P(r)e^{\pm j(l-1)\phi} \\ &+ (1-s)Q(r)e^{\pm j(l+1)\phi}]. \end{aligned} \tag{8}$$

$$\begin{aligned} OAM_y^{\pm} = &\pm \frac{j\beta A}{[k^2 n(r)^2 - \beta^2]}[(1+s)P(r)e^{\pm j(l-1)\phi} \\ &- (1-s)Q(r)e^{\pm j(l+1)\phi}]. \end{aligned} \tag{9}$$

$$\begin{aligned} \hat{\sigma}^{\pm} OAM^{\pm} = &- \frac{j\beta A}{[k^2 n(r)^2 - \beta^2]}[(\vec{x} \mp j\vec{y})(1+s)P(r) \\ &e^{\pm j(l+1)\phi} + (\vec{x} \pm j\vec{y})(1-s)Q(r)e^{\pm j(l-1)\phi}]. \end{aligned} \tag{10}$$

In order to prove the above conclusion, we compared OAM purity and intrinsic crosstalk properties of three different refractive index profiles of ring-core, which are shown in Figs. 9(a), 9(b), and 9(c). As the definition in Ref.[23],

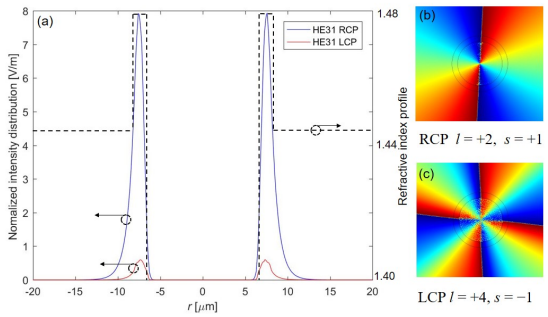

Figure 8: (a) Normalized intensity distribution of OAM mode formed by even and odd HE_{31} vector modes with $\pi/2$ phase shift in a strongly-guiding hollow ring-core fiber, where core inner radius is 6.4 μm, core outer radius is 8 μm, ring-core refractive index is 1.480, and refractive index of cladding is 1.444, and (b) phase front of the RCP content, $l = +2$, and (c) phase front of the LCP content, $l = +4$.

the purity is the power weight of the major OAM light in the all synthesized OAM lights and the intrinsic crosstalk can be calculated by 1-purity. In Figs. 9(d) and 9(e), solid lines with circles represent the OAM modes formed by even and odd HE mode with $\pi/2$ phase shift and solid lines with asterisks represent the OAM modes formed by even and odd EH mode with $\pi/2$ phase shift. In Figs. 9(d) and 9(e), solid lines in green stand for an one-layer hollow-ring-core fiber (OL-HRCF), whose core outer radius (a_{out}) is 8 μm, inner and outer radius ratio ($a_{\mathrm{in}}/a_{\mathrm{out}}$) is 0.8, core refractive index (n_{max}) at λ of 1550 nm is 1.480, cladding refractive index (n_{cl}) at λ of 1550 nm is 1.444, refractive index of inner-depressed part (n_{de}) is 1.0. Solid lines in red represent an two-layer hollow-ring-core fiber (TL-HRCF), whose a_{out} is 8 μm, first inner and outer radius ratio ($a_{\mathrm{in}}/a_{\mathrm{out}}$) is 0.8, second inner and outer radius ratio ($a_{\mathrm{mid}}/a_{\mathrm{out}}$) is 0.67, n_{max} at λ of 1550 nm is 1.480, n_{cl} at λ of 1550 nm is 1.444, n_{de} is 1.0. Solid lines in blue represent an two-layer solid-ring-core fiber (TL-SRCF), whose a_{out} is 8 μm, $a_{\mathrm{in}}/a_{\mathrm{out}}$ is 0.8, $a_{\mathrm{mid}}/a_{\mathrm{out}}$ is 0.67, n_{max} at λ of 1550 nm is 1.480, n_{cl} at λ of 1550 nm is 1.444, n_{de} at λ of 1550 nm is 1.444. Compared with OL-HRCF (green solid line), TL-HRCF (red solid line) take advantage of one more layer to enlarge the thickness of ring-core. As a result, OAM purity of

TL-HRCF is higher than that of OS-HRCF and intrinsic crosstalk of TL-HRCF is smaller than that of OL-HRCF. Compared with TL-HRCF (red solid lines), TL-SRCF (blue solid line) lifts the inner-depressed refractive index from 1.0 to 1.444. Since relative refractive index between core and cladding is decreased, the OAM mode purity of TL-SRCF is enhanced. Therefore, we can know that instead of increasing Δ_{co} constantly, adding more up-doping layer is a better way to enlarge the separation between CV eigenmodes and meanwhile maintain high mode purity.

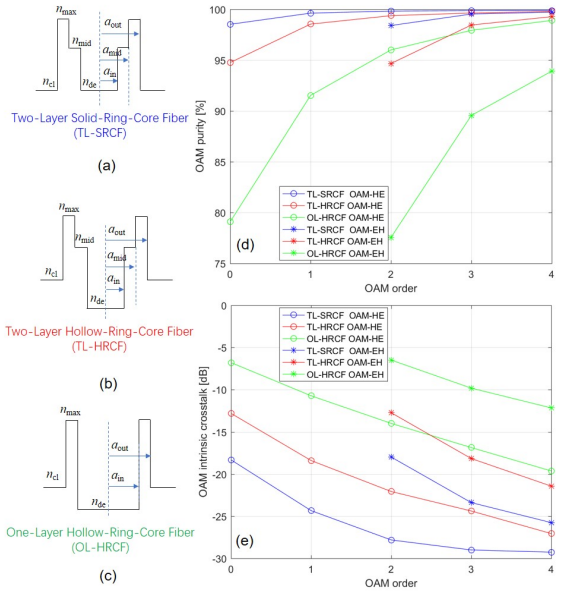

Figure 9: Comparison among of (a) TL-SRCF, (b) TL-HRCF, (c) OL-HRCF for (d) OAM purity and (e) intrinsic crosstalk properties.

4. Mode Group Supporting MM-RCF

For the above-mentioned strongly-guiding MM-RCF, it is hard to isolate so many CV eigenmodes with large enough $\Delta n_{\mathrm{eff,CV}}$, which is usually set at 1.0×10^{-4} [9]. However, if we consider the idea of mode group transmission,

larger mode number can be obtained. In this case, the CV eigenmodes with same value of l are allowed to degenerate with each other and the adjacent OAM mode groups have sufficient $\Delta n_{\mathrm{eff,MG}}$. Therefore, we can detect each mode group directly and take advantage of fixed 4×4 MIMO-DSP to demultiplex the coupled CV eigenmodes. In this section, we will discuss the design method for mode group supporting MM-RCF and figure out what the upper limit of mode group number is.

The fiber model we used for the calculation is the monolayer ring-core fiber as shown in Fig. 1(c). Fig. 10 illustrates cut-off line for each CV eigenmode as function of outer radius d and ratio ρ of inner and outer radii for the MM-RCF. The data in Fig. 10 were all obtained by using the theoretical calculating method described in Section II. Here, Δ_{co} is set at 1%, because higher doping content will cause large scattering loss. Take red solid line in Fig. 10 as an example, values of d and ρ chosen in the left region of the red solid line makes HE_{12} cut off, while the region at the right side of the red solid line includes the HE_{12} mode. Therefore, in order to suppress the radial higher-order modes, the core design region is the domain at top left of the red solid line. In Fig. 10, we can still know that ring-core need to be larger and thinner as mode number increases. As a result, if the mode number increase, the design region for the ring-core will becomes narrow and thickness of the ring-core need to be smaller. Therefore, maximum mode number is limited by the thickness of ring-core and the cut-off of the radial high-order mode. In order not to bring intrinsic crosstalk into the fiber, we set the upper limit of ρ as 0.8, so the maximum mode order can reach $l = 10$ for the case that $\Delta_{\mathrm{co}} = 1\%$.

As shown in Fig. 11, we take the mode order of $l = 8$ as an example to discuss the appropriate value selection for d and ρ. In Fig. 11, the green dashed line is the cut-off of HE_{91} mode, the black dashed line is the cut-off of $\mathrm{HE}_{10,1}$ mode, and the red solid line is the cut-off of HE_{12} mode. The region surrounded by these three lines is the core design region for the OAM modes with $l = 8$. For the adjacent mode groups, the $|\Delta n_{\mathrm{eff,MG}}|$ between the low-order OAM mode groups is smaller than that between the high-order OAM mode groups, which

can also be told in Fig. 7. For the degenerated CV eigenmodes, we should make the differential mode delay (DMD) as small as possible and the DMD is larger in the high-order mode group than in low-order mode group. Therefore, we take four points in Fig. 11 to analyze the changing trench of $|\Delta n_{\mathrm{eff,MG}}|$ between OAM_{01} and OAM_{11} ($|\Delta n^{*}_{\mathrm{eff,MG}}|$) and DMD between HE_{91} and EH_{71} (DMD^{*}) in OAM mode group with $l = 8$. The values of (d, ρ) of four points are (14.6,0.78), (15, 0.75), (15.4, 0.78), and (15, 0.81), respectively. It can be found that if d and ρ decrease, larger $|\Delta n^{*}_{\mathrm{eff,MG}}|$ can be obtained, while if d and ρ increase, smaller DMD^{*} can be got. Hence, there is a tradeoff relationship between $|\Delta n_{\mathrm{eff,MG}}|$ and HE/EH mode DMD in the mode group. It should be noted that above-mentioned up-doping inner layer is suggested to be added to ensure the mode purity if the thickness becomes very thin.

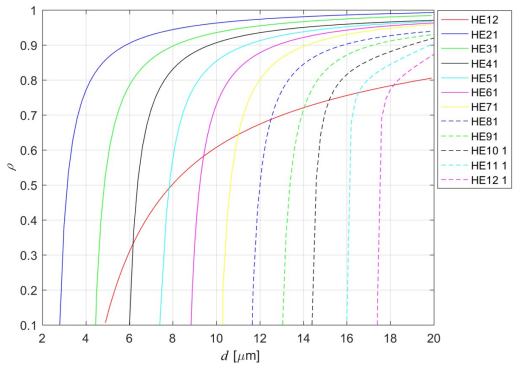

Figure 10: Cut-off line for each CV eigenmode as function of outer radius d and ratio of inner and outer radii ρ for the MM-RCF, where Δ_{co} is 1%, n_{cl} is 1.444 and λ is 1550 nm.

5. Conclusion

This paper mainly analyzed the mode properties for OAM-carrying fibers. Firstly, we explained why OAM-carrying fiber usually has ring-type core in detail and made the theoretical modeling for the ring-core fiber, which can get

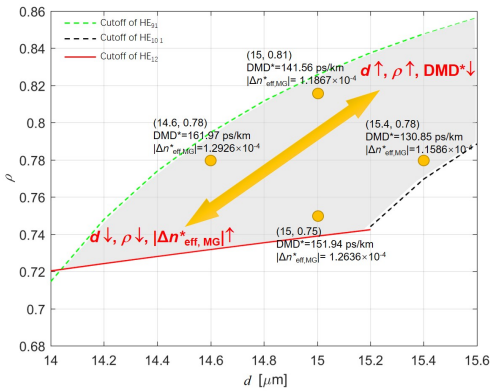

Figure 11: Design region of d and ρ for OAM mode with $l = 8$, where Δ_{co} is 1%, n_{cl} is 1.444 and λ is 1550 nm.

the propagation constant for each CV eigenmode quickly. Secondly, according to the separation degree of CV eigenmodes, MM-RCF can be divided into two types. The one is called strongly-guiding MM-RCF, where each CV eigenmode are isolated. Larger Δ_{co} and larger ρ can obtain larger separation between CV eigenmodes. However, it will cause strong spin-orbital coupling. It has been proven that adding more up-doping layers can enhance the separation of CV eigenmodes and meanwhile decrease the intrinsic crosstalk. The other MM-RCF is mode group supporting fiber, where neighboring OAM mode groups are separated but the CV eigenmodes with same order are degenerated. The maximum mode number is limited by thickness of ring-core and the cut-off of the radial higher-order mode. The tradeoff relationship between $|\Delta n_{\mathrm{eff,MG}}|$ and DMD in the mode group has been revealed in this paper. The mode properties discussed in this paper can give some guidance for the design of multi-mode ring-core fiber.

6. Acknowledgments

This research was sponsored by National Key R&D Program of China 2019YFA0706300 from Ministry of Science and Technology, China; National Natural Science Foun-

dation of China (NSFC) (Grant No. U2001601, U1701661); Guangzhou basic and applied basic research foundation (Grant No. 202002030327).

References

[1] G. Li, N. Bai, N. Zhao, C. Xia, Space-division multiplexing: the next frontier in optical communication, Adv. Opt. Photon. 6 (4) (2014) 413–487. doi:10.1364/AOP.6.000413.

[2] D. J. Richardson, J. M. Fini, L. E. Nelson, Space-division multiplexing in optical fiber, Science 7 (2013) 354–362.

[3] K. Saitoh, S. Matsuo, Multicore fiber technology, J. Lightwave Technol. 34 (1) (2016) 55–66.

[4] J. Wang, Y.-Y. Yang, I. M. Fazal, N. Ahmed, Y. Yan, H. Huang, Y. Ren, Y. Yue, S. Dolinar, M. Tur, A. E. Willner, Terabit free-space data transmission employing orbital angular momentum multiplexing, Nature Photonics 6 (2012) 488–496.

[5] Y. Yan, G. Xie, M. Lavery, H. Huang, N. Ahmed, C. Bao, Y. Ren, Y. Cao, L. Li, Z. Zhao, A. Molisch, M. Tur, M. Padgett, A. Willner, High-capacity millimetre-wave communications with orbital angular momentum multiplexing, Nature Communications 5 (2014) 4876.

[6] N. Bozinovic, Y. Yue, Y. Ren, M. Tur, P. Kristensen, H. Huang, A. E. Willner, S. Ramachandran, Terabit-scale orbital angular momentum mode division multiplexing in fibers, Science 340 (6140) (2013) 1545–1548. arXiv:https://science.sciencemag.org/content/340/6140/1545.full.pdf, doi:10.1126/science.1237861.

[7] Z. Xie, S. Gao, T. Lei, S. Feng, Y. Zhang, F. Li, J. Zhang, Z. Li, X. Yuan, Integrated (de)multiplexer for orbital angular momentum fiber communication, Photon. Res. 6 (7) (2018) 743–749.

[8] J. Ma, F. Xia, S. Chen, S. Li, J. Wang, Amplification of 18 oam modes in a ring-core erbium-doped fiber with low differential modal gain, Opt. Express 27 (26) (2019) 38087–38097.

[9] C. Brunet, B. Ung, P. Bélanger, Y. Messaddeq, S. LaRochelle, L. A. Rusch, Vector mode analysis of ring-core fibers: Design tools for spatial division multiplexing, Journal of Lightwave Technology 32 (23) (2014) 4648–4659. doi:10.1109/JLT.2014.2361432.

[10] S. Ramachandran, P. Kristensen, M. F. Yan, Generation and propagation of radially polarized beams in optical fibers, Opt. Lett. 34 (16) (2009) 2525–2527. doi:10.1364/OL.34.002525.

[11] B. Ung, P. Vaity, L. Wang, Y. Messaddeq, L. A. Rusch, S. LaRochelle, Few-mode fiber with inverse-parabolic graded-index profile for transmission of oam-carrying modes, Opt. Express 22 (15) (2014) 18044–18055.

[12] P. Gregg, P. Kristensen, S. Ramachandran, Conservation of orbital angular momentum in air-core optical fibers, Optica 2 (3) (2015) 267–270.

[13] C. Brunet, P. Vaity, Y. Messaddeq, S. LaRochelle, L. A. Rusch, Design, fabrication and validation of an oam fiber supporting 36 states, Opt. Express 22 (21) (2014) 26117–26127. doi:10.1364/OE.22.026117.

[14] A. Tandjè, J. Yammine, M. Dossou, G. Bouwmans, K. Baudelle, A. Vianou, E. R. Andresen, L. Bigot, Ring-core photonic crystal fiber for propagation of oam modes, Opt. Lett. 44 (7) (2019) 1611–1614.

[15] J. Tu, Z. Liu, S. Gao, Z. Wang, J. Zhang, B. Zhang, J. Li, W. Liu, H. Tam, Z. Li, C. Yu, C. Lu, Ring-core fiber with negative curvature structure supporting orbital angular momentum modes, Opt. Express 27 (15) (2019) 20358–20372. doi:10.1364/OE.27.020358.

[16] J. Tu, S. Gao, Z. Wang, Z. Liu, W. Li, C. Du, W. Liu, Z. Li, C. Yu, H. Tam, C. Lu, Bend-insensitive grapefruit-type holey ring-core fiber for weakly-

coupled oam mode division multiplexing transmission, Journal of Lightwave Technology 38 (16) (2020) 4497–4503. doi:10.1109/JLT.2020.2987328.

[17] L. Zhu, A. Wang, S. Chen, J. Liu, Q. Mo, C. Du, J. Wang, Orbital angular momentum mode groups multiplexing transmission over 2.6-km conventional multi-mode fiber, Opt. Express 25 (21) (2017) 25637–25645. doi:10.1364/OE.25.025637.

[18] J. Zhang, J. Liu, L. Shen, L. Zhang, J. Luo, J. Liu, S. Yu, Mode-division multiplexed transmission of wavelength-division multiplexing signals over a 100-km single-span orbital angular momentum fiber, Photon. Res. 8 (7) (2020) 1236–1242. doi:10.1364/PRJ.394864.

[19] A. R. May, M. N. Zervas, Few-mode fibers with improved mode spacing, in: 2015 European Conference on Optical Communication (ECOC), 2015, pp. 1–3. doi:10.1109/ECOC.2015.7341706.

[20] K. Okamoto, Fundamentals of Optical Waveguides, Elsevier, 2006.

[21] A. W. Snyder, J. D. Love, Optical Waveguide Theory, Chapman and Hall, 1983.

[22] L. Wang, A. Corsi, L. A. Rusch, S. LaRochelle, Investigation of orbital angular momentum mode purity in air-core optical fibers, in: 2016 IEEE Photonics Society Summer Topical Meeting Series (SUM), 2016, pp. 203–204. doi:10.1109/PHOSST.2016.7548809.

[23] Z. Zhang, J. Gan, X. Heng, Y. Wu, Q. Li, Q. Qian, D. Chen, Z. Yang, Optical fiber design with orbital angular momentum light purity higher than 99.9%, Opt. Express 23 (23) (2015) 29331–29341. doi:10.1364/OE.23.029331.